Available online at www.sciencedirect.com
SCIENCE DIRECT®
Computers and Geotechnics 31 (2004) 559–573
COMPUTERS AND GEOTECHNICS
www.elsevier.com/locate/compgeo

Time-dependent deformation in high concrete-faced rockfill dam and separation between concrete face slab and cushion layer

Bingyin Zhang [a], J.G. Wang [b,*], Ruifeng Shi [a]

[a] Department of Hydraulic Engineering, Tsinghua University, Beijing 100084, China
[b] Tropical Marine Science Institute, National University of Singapore, 10 Kent Ridge Crescent, Singapore 119260, Singapore

Received 12 January 2004; received in revised form 8 July 2004; accepted 27 July 2004
Available online 14 October 2004

Abstract

The contact behavior between concrete face slab and dam body is important to the safety of concrete-faced rockfill dams. The deficient of dam body and the separation of concrete slab from cushion layer during construction and in operation are the main concerns. This paper proposes a contact analysis method to study the effect of non-linearity and time-dependent deformation on the separation and the deficient. This contact analysis method regards dam body and concrete slab as two independent deformable bodies. These two deformable bodies follow Coulomb friction law at contact interface when they contact each other. The rockfill materials in dam body are assumed to be non-linear and time-dependent but concrete slab is elastic. As an example, a high concrete-faced rockfill dam of Tianshengqiao-I in China is numerically analyzed, and the numerical results are compared with in situ measurements. The results reveal that whether the deformation of dam body is non-linear or time-dependent, this contact analysis method can effectively simulate the separation between concrete slab and cushion layer without the drawbacks of interface element methods.

Keywords: High concrete-faced rockfill dam; Concrete face slab; Contact analysis; Finite element method; Non-linearity; Creep deformation; Separation

1. Introduction

Concrete-faced rockfill dam (CFRD) is quickly developed in recent decades [1] due to its good adaptability to topography, geology and climate and easily available construction materials. China constructs higher and higher CFRDs in recent years. For example, Tianshengqiao-I CFRD (called as TSQ-I CFRD later) is 178 m high. It locates on the Nanpan river in southwestern China and is the highest CFRD in China so far. Construction of such a high CFRD confronts some technical problems during construction and in operation stage: the deficient of dam body and the separation of concrete face slab from cushion layer. The separation may produce major cracks in the concrete face slab and thus reduce the safety factor due to seepage failure [2]. Post-failure investigation [3] reveals that leakage-induced failure is a serious issue not only for CFRDs but also for concrete dams. In order to avoid this potential risk in high CFRDs, it is necessary to understand the mechanisms for the deficient of dam body and the separation of concrete face slabs from cushion layer.

The separation of concrete face slab from cushion layer is inevitable due to the difference settlement or deformation of dam body and concrete slabs [4]. This separation is not salient when the stress level in dam body is low. With the increase of dam height, the stress level increases and the deformation of rockfill materials becomes strongly non-linear and time-dependent. These mainly contribute the deficient of dam body and thus

* Corresponding author. Tel.: +65 6874 6591; fax: +65 6779 1635.
E-mail address: tmswjg@nus.edu.sg (J.G. Wang).

0266-352X/$ - see front matter © 2004 Elsevier Ltd. All rights reserved.
doi:10.1016/j.compgeo.2004.07.004

cause the separation of concrete face slabs from cushion layer. How the non-linear and time-dependent deformation induces the separation has not been well studied for high CFRDs. This paper focuses on the effects of non-linearity and time-dependent deformation of rockfill materials on the deficient and the separation for TSQ-I CFRD. Being different from the conventional FEM with interface element [5], a contact analysis method is proposed in this paper. This contact analysis method regards concrete face slab and dam body as two independent deformable bodies. When the two bodies contact each other, contact mechanics [6] is applied to treat the interface, thus the slab can separate from cushion layer without the limitation of small deformation.

Contact analysis is of highly non-linearity. When two deformable bodies contact, the contacting part or interface is movable with loading. The physical and mechanical properties at the interface may be non-linear or elastoplastic [7], too. The numerical algorithm for contact analysis should accurately track the motion of multiple bodies and detect their movable interface in each loading increment. Therefore, contact analysis is to detect the motion of bodies, apply constraints along interface to avoid penetration and apply appropriate dynamic conditions to simulate the frictional property of rough interfaces.

Several methods have been proposed to treat contact problems such as augmented Lagrangian methods [8], penalty methods or interface element [5,9] and direct constraints method [6]. Lagrangian multiplier technique is the most elegant algorithm to implement mathematical constraints. However, Lagrangian multiplier introduces a non-positive definite system even for well-posed physical problems due to diagonal zeros. This imposes additional numerical difficulties in computational procedure [10]. Interface elements are widely employed to describe the contact properties in geotechnical problems [5,11–15]. Interface element is based on continuum mechanics [7] and described by node pairs. This imposes some limitations on the relative motion of bodies. For example, interface element cannot describe the discontinuity at large slide or separation. Direct constraints method is the best choice. When contact occurs, kinematic and dynamic constraints are imposed as direct constraints. This method is accurate if the contact can be accurately detected. In addition, direct constraints method can include complex contact conditions at any time and at any location. Because no interface element is used in this method, the node distribution on both sides of the interface may not match.

This paper proposes a contact analysis method to describe the contact behavior of concrete slab and rockfill dam body. This contact analysis method regards concrete slab and rockfill dam body as independent deformable continuums. The contact parts between concrete slab and rockfill dam body may be in contact or detaching but without penetration. The separation magnitude has no limitation such as small deformation, and the friction properties along the interface are easily implemented. Furthermore, rockfill materials may be linear or non-linear and creep. With this contact analysis method, this paper will study the deficient of dam body and the separation of the concrete slab from the cushion layer for the TSQ-I dam at both construction and operation stages. The numerical results are compared with in situ measurements. The focus is on the effect of non-linearity and creep deformation on the deficient of dam body and the separation of concrete slab from cushion layer.

This paper is organized as follows: Section 2 presents a direct constraint model for two deformable bodies. Section 3 briefs the constitutive models used for rockfill dam body and concrete slab. Duncan EB model [16] is employed to describe the non-linearity of rockfill materials and an empirical creep model [17] is used to describe the time-dependent or creep deformation. Section 4 outlines the main features of TSQ-I CFRD in China and in situ observations. Section 5 numerically studies the effect of non-linear and time-dependent deformation on the deficient and the separation at different construction phases. Numerical results are compared with in situ measurements. The mechanisms for the separation are analyzed. Section 6 draws conclusions and recommendations for future design and construction of high CFRDs.

2. Direct constraint model

2.1. Contact analysis method

This problem occupies domain Ω which is composed of sub-domains Ω_1 (bounded by Γ_1) and Ω_2 (bounded by Γ_2) as shown in Fig. 1. When the two bodies contact, their potential contacting boundary is Γ_{1p} in Γ_1 and Γ_{2p} in Γ_2. These potential contacting boundaries can be prescribed to reduce the search time in computation. Based on virtual work principle of elasticity, a discrete

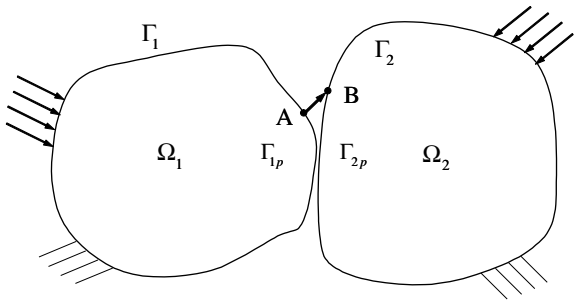

Fig. 1. Contact of two deformable bodies.

system equation in each sub-domain is obtained as follows:

$$K_{11}u_1 + K_{12}u_{12} = f_1 \quad \text{for} \quad \Omega_1, \tag{1}$$

$$K_{22}u_2 + K_{21}u_{21} = f_2 \quad \text{for} \quad \Omega_2, \tag{2}$$

where u_1 and u_2 are the displacement increments in Ω_1, Ω_2 and the boundaries except potential contacting ones. u_{12} is the displacement increment along Γ_{1p} and u_{21} is the one along Γ_{2p}.

When the two bodies are not in contact, any deformable body has no constraint on the other, thus Eqs. (1) and (2) are independent each other. The displacement increments u_1 and u_{12} are solved from Eq. (1) while u_2 and u_{21} are determined by Eq. (2).

When the two bodies are in contact, one deformable body imposes constraints on the other. At this time, u_{12} and u_{21} are no independent any more. The potential contacting boundaries may be partially or fully constrained. At this time, kinematic and dynamic constraints conditions should be imposed along the interface. As shown in Fig. 1, if point A on Γ_{1p} is coincided with point B on Γ_{2p}, the kinematic constraint is generally expressed as

$$\left(u_{12}^{A} - u_{21}^{B}\right)n \leqslant \text{TOL}, \tag{3}$$

where n is the directional cosine of the contact point, and TOL the closure distance or contact tolerance. The dynamic condition is Coulomb's friction law in our computation

$$f_t \leqslant -\mu \cdot f_n \cdot t, \tag{4}$$

where f_t is the tangential friction force, f_n the normal force, μ the friction coefficient and t the tangential vector which is in the direction of relative velocity.

The numerical procedure is shown in Fig. 2 for this contact analysis method. This procedure includes the definition of contact bodies, the detection of contact, the implementation of constraints, the model of friction, the change of contact constraints, the checking of constraints and judgment of separation and penetration. This procedure is completed through a non-linear algorithm such as improved Newton–Raphson scheme.

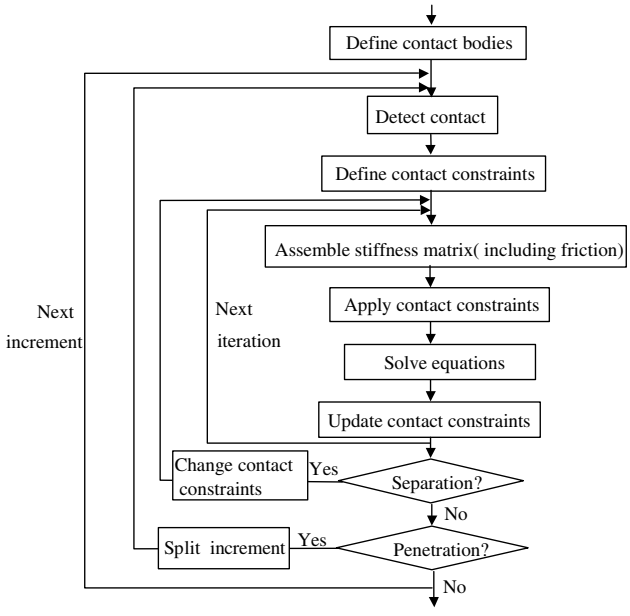

Fig. 2. Numerical procedure for direct constraints method.

2.2. Contact deformation and forces of two contact elements

When two deformable bodies contact each other, a multipoint constraint is automatically imposed. Because the deformable bodies have been discretized into elements, the contact of bodies becomes the contact of elements as shown in Fig. 3. This is a typical node-edge contact mode. In FEM, the edge displacement of an element can be completely expressed by nodal displacements through point interpolation method [18]. Because node 1 in the element A is contacting with the 5-6 edge of the element B, its displacement increment is expressed by the displacement increments of 5-6 edge if linear interpolation is employed

$$\Delta\bar{u}_1 = 0.5(1-\xi)\Delta\bar{u}_5 + 0.5(1+\xi)\Delta\bar{u}_6, \tag{5}$$

where ξ is the natural coordinate of 5-6 edge and Δ denotes increment.

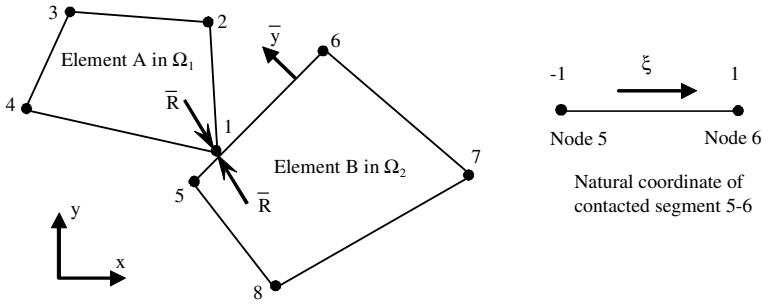

Fig. 3. Local contact between two deformable elements.

Contact force $\bar{R}$, its components are (f_n, f_t), exerts on the contact point 1. This force as an unknown is incorporated into the Eqs. (1) and (2), thus the set of equations include Eqs. (1), (2), and (5). In this set of equations, the unknowns are the displacement increments in Eqs. (1) and (2) as well as the contact force $\bar{R}$. They can be completely solved.

Above set of equations is strongly non-linear due to sliding and reopening of interface. When the interface slides, the friction law of Eq. (4) is imposed. When the contact reopens or re-closes up, a strongly non-linear equation is introduced. The current contact analysis method employs an iteration procedure to solve this non-linear equation. In computation, potential contact interface is treated as follows: When contact is detected, a reaction force $\bar{R}$ is given at the contact. This reaction force $\bar{R}$ is used to balance the internal stress of the elements adjacent to this node. When the contact is detected to be open in iteration, this reaction force does not exist. The previous force will be used as a residual force and redistributed in the deformable body. Such an iteration procedure can achieve a new equilibrium state.

2.3. Detection of contact

Detection of contact is an important issue to affect the computational efficiency of this contact analysis method. In order to improve computational efficiency, incremental procedure is used in computation and the potential contact boundaries are prescribed. Those nodes on the potential contact boundaries are called as potential contact nodes. Each iteration will check every potential contact node to determine whether it falls within a contact segment or not. If potential contact nodes and segments are huge, the efficiency of contact detections is a big problem. In order to speed up this search process, a bounding box algorithm or bucket algorithm [19] is employed in computation. This algorithm groups the potential contact nodes and first checks whether a node is near a group or not. This can quickly determine the relation of a node and a segment. If the node falls within the bounding box, the search is finely tuned to determine its exact status. It is noted that numerical analysis uses the contact tolerance in Eq. (3) to justify the contact status. A node is regarded as in contact with a segment when that node is within the contact tolerance.

3. Constitutive models for dam materials

In this computation, concrete face slab is modeled as linear elastic material with Young's modulus and Poisson ratio. No failure is allowed. However, rockfill materials are modeled by Duncan EB model [16] (called as EB model hereafter).

3.1. Outline of EB model

EB model adopts incremental Hooke's law to describe the non-linearity of rockfill materials and Mohr-Coulomb's law to model the shear failure. This model uses two moduli, deformation modulus E_t and bulk modulus B, which are determined by following hyperbolic stress–strain curve

$$\sigma_1 - \sigma_3 = \frac{\varepsilon_1}{a + b\varepsilon_1}, \tag{6}$$

where $(\sigma_1 - \sigma_3)$ is deviatoric stress, and the ε_1 is the corresponding strain. a and b are soil parameters.

The deformation modulus of E_t is then obtained from Eq. (6)

$$E_t = E_i \left[1 - R_f \frac{(1-\sin\phi)(\sigma_1 - \sigma_3)}{2c\cdot\cos\phi + 2\sigma_3 \sin\phi}\right]^2, \tag{7}$$

where c is cohesion intercept, ϕ the angle of internal friction, and R_f a failure ratio. The E_i, initial deformation modulus, expresses the compression-hardening property of rockfill materials

$$E_i = k \cdot P_a \left(\frac{\sigma_3}{P_a}\right)^n, \tag{8}$$

where P_a is the standard atmospheric pressure, k and n are soil constants.

For rockfill materials, the cohesion intercept c is generally taken as zero. However, the angle of internal friction ϕ changes with compression stress

$$\phi = \phi_0 - \Delta\phi \log\left(\frac{\sigma_3}{P_a}\right), \tag{9}$$

where ϕ_0 and $\Delta\phi$ are two constants for soil strength.

The bulk modulus B has following form:

$$B = k_b P_a \left(\frac{\sigma_3}{P_a}\right)^m, \tag{10}$$

where k_b and m are soil constants.

3.2. Creep model for rockfill materials

The empirical creep model in [17] is employed in this paper. This model assumes that creep strain ε_t increases exponentially with time t

$$\varepsilon_t = \varepsilon_f (1 - e^{-\alpha t}), \tag{11}$$

where ε_f is the ultimate total creep strain. This creep strain ε_t is decomposed into volumetric strain ε_v and shear strain γ. They have following forms:

$$\dot{\varepsilon}_v = \alpha\varepsilon_{vf}\left(1 - \frac{\varepsilon_{vt}}{\varepsilon_{vf}}\right), \quad \dot{\gamma} = \alpha\gamma_f\left(1 - \frac{\gamma_t}{\gamma_f}\right), \tag{12}$$

$$\varepsilon_{vf} = b\left(\frac{\sigma_3}{P_a}\right)^m, \quad \gamma_f = d \cdot \frac{s_L}{1 - s_L}, \tag{13}$$

where ε_{vf} and γ_f are ultimate total volumetric and shear strains, respectively. b, d and m are material parameters, s_L is the stress level which is

$$s_L = \frac{(1 - \sin\phi)(\sigma_1 - \sigma_3)}{2c \cdot \cos\phi + 2\sigma_3 \sin\phi}. \tag{14}$$

If the principal axes of strain and stress are coaxial, the strain rate is expressed as

$$\{\dot{\varepsilon}\} = \frac{1}{3}\dot{\varepsilon}_v\{I\} + \frac{\dot{\gamma}}{\sigma_s}\{s\}, \tag{15}$$

where I is a unit vector, $s_{ij} = \sigma_{ij} - \frac{1}{3}\sigma_{kk}\delta_{ij}$ the deviatoric stress tensor, and σ_s an equivalent stress which is defined

$$\sigma_s = \frac{1}{\sqrt{2}}\sqrt{(\sigma_1 - \sigma_2)^2 + (\sigma_2 - \sigma_3)^2 + (\sigma_3 - \sigma_1)^2}. \tag{16}$$

Initial strain technique [20] is used to implement this creep model. The time history is divided into several increments Δt and ε_{vt} and γ_t is obtained through summation

$$\varepsilon_{vt} = \sum \dot{\varepsilon}_v \Delta t, \quad \gamma_t = \sum \dot{\gamma} \Delta t. \tag{17}$$

4. TSQ-I concrete-faced rockfill dam project and in situ observations

4.1. Project outline

Tianshengqiao-I hydropower project (TSQ-I project) is on the Nanpan river in southwestern China. The project layout is shown in Fig. 4. Its water retaining structure is a concrete-faced rockfill dam. This dam is 178 m high and 1104 m long. The rockfill volume of the dam body is about 18 million m^3 and the area of the concrete face is 173,000 m^2. A surface chute spillway on the right bank allows a maximum discharge of 19,450 m^3/s. The tunnel in the right abutment is for emptying reservoir in operation. Left abutment has four power tunnels and a surface powerhouse with a total capacity of 1200 MW.

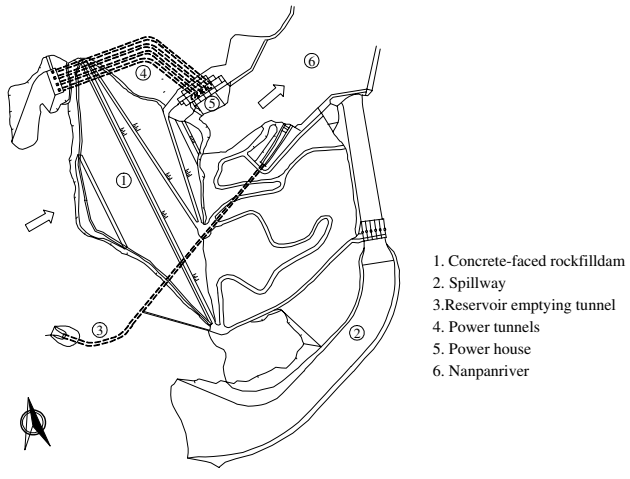

Fig. 4. Project layout of Tianshengqiao-I concrete-faced rockfill dam.

4.2. Material zones and construction phases

A typical cross-section is shown in Fig. 5(a). The slope is 1:1.4 at upstream and 1:1.25 at downstream. There are two 10 m wide access berms at the downstream. Table 1 lists the main parameters of fillings. The bedding zone IIA has horizontal thickness of 3.0 m and is of low permeability. This layer is used as a semi-pervious layer during diversion sequence before casting concrete face slab. A transition zone (also denoted as IIIA) with a horizontal width of 5.0 m is provided between bedding zone and rockfill zone. This can prevent fine particles of the bedding zone from entering the pores of the rockfill. The rockfill zone IIIB at the upstream is the main part of dam body. It provides a support for hydrostatic loads transmitted from the bedding zone and transition zone. The rockfill zone IIID at the downstream is filled with relatively poor quality materials since this zone bears smaller load than zone IIIB. Weathered and fresh mudstone and sandstone from the excavation of spillway fills the zone IIIC, which is above the water level in the downstream area.

The upstream concrete face was divided into 69 slabs with vertical joints in 16 m spacing. The thickness of the slab is 0.3 m at the top elevation of 787.3 and 0.9 m at the bottom elevation of 616.5 m, with a varying relationship $d = 0.3 + 0.0035H$, where d is the thickness of the slab and H the vertical distance below the top elevation 787.3 m. The reinforcement is placed in the center part of the slab. The steel ratio is 0.4% along slope and 0.3% in the horizontal direction. The concrete has middle strength but high seepage resistance.

Fig. 5(b) shows the construction phases and Table 2 gives the construction time of each phase. The dam construction commenced in February 1996, and completed in March 1999 for dam body and in May 1999 for face slabs. Construction stages were planned according to river diversion and utilization of materials from excavations. Five blocks were formed at the elevation of El.682 m, El.725 m, El.748 m, El.768 m and El.791 m. The concrete slab was cast in three phases. Their top elevations are El.680 m, El.746 m and El.787.3 m. The impounding water level reached El.768 m in August 1999.

4.3. Observation on separation

A complete monitoring system was installed to monitor the deformation of dam body in both construction and operation stages. This system also measures the

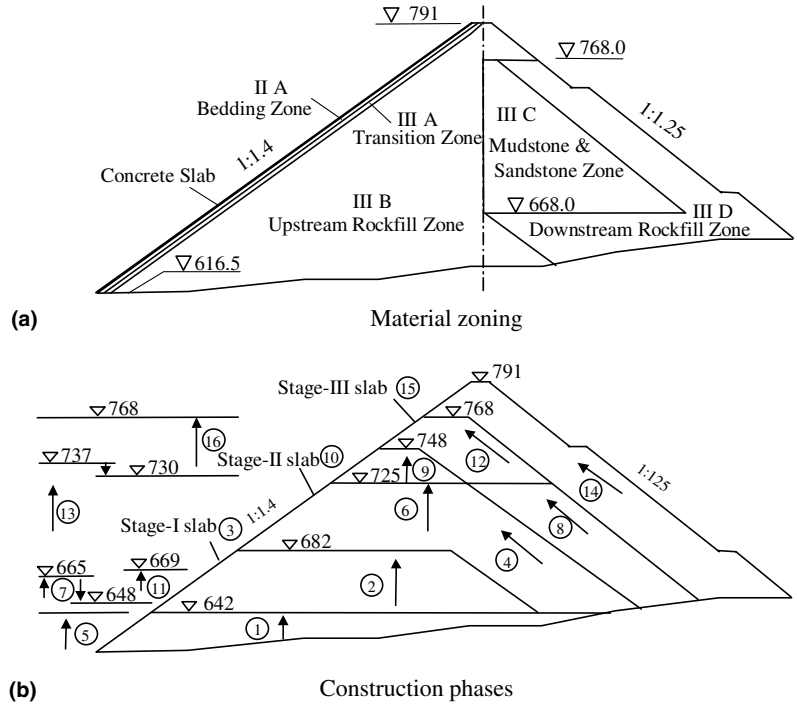

Fig. 5. Material zones and construction phases of TSQ-I CFRD.

Table 1
Design parameters of dam materials

Material no.	Material description	Maximum particle size (cm)	Dry unit weight (kN/m^3)	Void ratio (%)
IIA	Processed limestone	8	22.0	19
IIIA	Limestone	30	21.5	21
IIIB	Limestone	80	21.2	22
IIIC	Mudstone and sandstone	80	21.5	22
IIID	Limestone	160	20.5	24

separation of concrete face slab from cushion layer. Fig. 6 shows the layout of instrument for monitoring the openings between slabs and cushion layer. Nine observation points on Sections 0 + 438 m, 0 + 662 m and 0 + 918 m were selected to observe the relative displacement between face slab and cushion layer.

Table 2
Construction phase and time

Filling step	Time	Remark
①	1996.01–1996.06	Fill dam body
②	1996.07–1997.02	Fill dam body
③	1997.03–1997.05	Cast Phase 1 concrete slab
④&⑥	1997.02–1997.10	Fill dam body
⑤	1997.05–1997.05	Water level rises
⑦	1997.06–1997.10	Water level fluctuation
⑧&⑨	1997.11–1998.01	Fill dam body
⑩	1997.12–1998.05	Cast Phase 2 concrete slab
⑪	1997.11–1997.12	Water level rises
⑫	1998.02–1998.08	Fill dam body
⑬	1998.06–1998.07	Water level rises
⑭	1998.08–1999.01	Fill dam body
⑮	1999.01–1999.05	Cast Phase 3 concrete slab
⑯	1999.06–1999.09	Store water

Fig. 7 shows the distribution of the openings between slabs and dam body. When preparing the slope face for stage-II slab, the constructed cushion layer was observed to be largely below the designed slope due to dam settlement. The maximum deficient reached 43 cm at the riverbed section. In addition, at the top area of the stage-I slab, the separation of the slab from the cushion layer was observed with the opening of 350 m in length (from slab number L14 to R8). Maximum opening reached 15 cm in width, 6.8 m in depth and took place in the middle of the riverbed section. The opening gradually decreased near left and right banks. Similar phenomena were also observed in subsequent construction stages. The maximum deficient of stage-III cushion still reached 78.4 cm although originally the cushion layer had an extra-fill of 25 cm in thickness. The separation of stage-II slab from the cushion layer reached 720 m long (from L27 to R18) and maximally 10 cm wide and 4.7 m deep. The stage-III slab

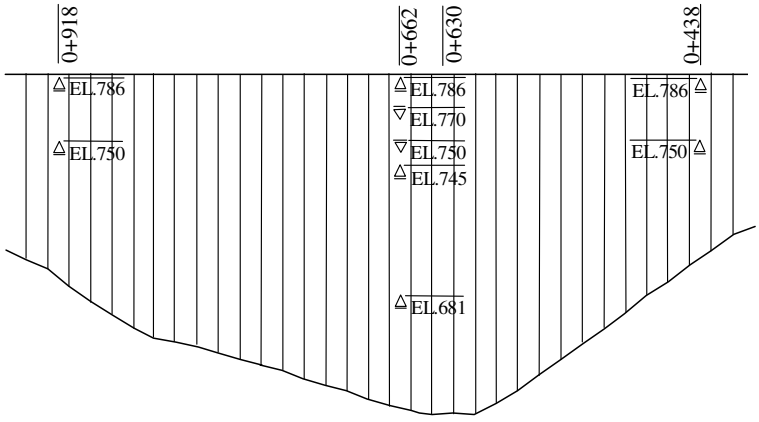

Fig. 6. Instrument layout for monitoring the openings between slabs and cushion layer.

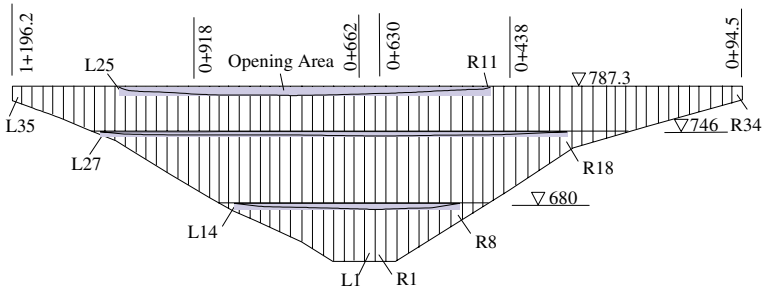

Fig. 7. In situ measured openings distribution in whole dam.

was also separated from the cushion layer and the opening was 610 m long (from L25 to R11) and maximally 15 cm wide and 10 m deep. Being different from the separation at stage-I and stage-II, the separation at stage-III occurred in the riverbed and left bank sections while the maximum opening occurred at a section in the left bank. The opening at section 0 + 630 m (in the middle of the riverbed) is only 3.5 cm wide and about 10 m deep on February 28, 2000. Such a separation has caused concentrative cracks in the face slabs near the bottom of the separation areas [21]. The crack width increased with further deformation of dam body. This is harmful to the anti-seepage function of the face slabs, thus endangering the dam safety.

5. Numerical analysis

5.1. Computational model and procedure

A two-dimensional finite element analysis was conducted. The separation of the concrete slab from the cushion and the deficient of dam body in TSQ-I dam are studied. We take the maximum cross-section (Section 0 + 630 m) for computation. This section is located in the middle of the riverbed and is also the major section monitored. Finite element model, as shown in Fig. 8, has 402 dam elements and 46 concrete face elements. Most of the elements are isoparametric quadratic elements but some triangular elements are used in the transition zone. Dam body, stage-I slab, stage-II slab and stage-III slab were considered as four deformable contact bodies. The contact tolerance between concrete face slabs and dam body was taken as 1 mm and their frictional coefficient was taken as 0.3. Because face slabs were well connected at different stages, the slabs have no physical interface. We use 'a glue model' along the interface [22]. That is, we use the same displacements and stress conditions along two sides of the interface. However, the nodes on both sides are not necessary to be identical or matching in our computation. Dam base is hard gray rock and its deformation monitored is very small, thus being ruled out from the monitored data. Therefore, this computational model sets fixed displacements along the rock base. The dam is located in a wide valley (crest length/dam height equals to 6.4), thus three-dimensional effect is negligible. The concrete face slab has Young's modulus of 3×10^4 MPa and Poisson ratio of 0.2. Table 3 lists the computational parameters of EB model and Table 4 lists the parameters of creep model

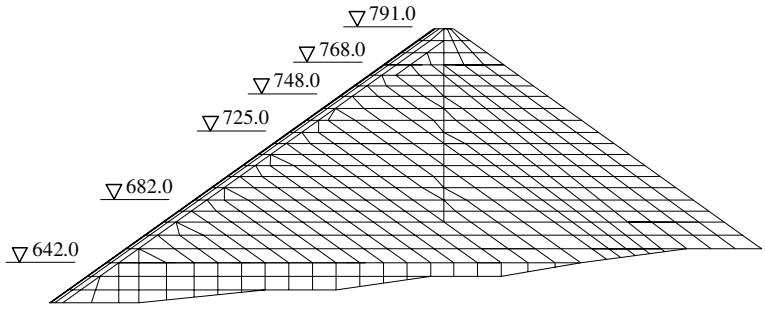

Fig. 8. A two-dimensional finite element mesh.

Table 3
EB model parameters of rockfill materials

Material no.	Density (kg/m^3)	ϕ_0 (°)	$\Delta\phi$ (°)	k	n	R_f	k_b	m
IIA	2200	50.6	7.0	1050	0.35	0.71	480	0.24
IIIA	2100	52.5	8.0	970	0.36	0.76	440	0.19
IIIB	2100	54.0	13.0	940	0.35	0.85	340	0.18
IIID	2050	54.0	13.5	720	0.30	0.80	800	−0.18
IIIC	2150	48.0	10.0	500	0.25	0.73	250	0.00

Table 4
Creep model parameters of rockfill materials

	IIA	IIIA	IIIB	IIID	IIIC
α	0.0035	0.0035	0.0035	0.0036	0.0038
b	0.0090	0.0090	0.0095	0.0100	0.0120
d	0.0021	0.0021	0.0021	0.0029	0.0025
m	0.38	0.38	0.38	0.38	0.38

for rockfill materials. The parameters of EB model are determined by laboratory tests and those of creep model are determined by a back analysis of in situ measurements at several points [17].

Computational procedure follows the construction sequence as shown in Fig. 5(b). Following treatment is used to compute the deficient and the separation. For example, we first simulate the blocks ① and ② of dam body up to El.682 m as shown in Fig. 5(b). In each block, layer-by-layer elements are reactivated to simulate the construction process. In each layer, mid-point stiffness is used for the non-linear constitutive model and computation is iterated until an energy error is tolerable. Impounding process is simulated by increasing 10 m water level each increment. Because stage-I concrete slab just cast, it should strictly contact with the upstream slope of El.682 m. We set the calculated displacements of dam body as zeros and keep the calculated stresses of the dam body. Then activate the elements of stage-I slab and continue to simulate dam construction until El.748 m (after construction phase ⑨ in Fig. 5(b) and before the construction of stage-II slab). The separation between stage-I face slab and dam body as well as the deficient at the upstream slope for stage-II face slab were acquired. The same procedure is repeated until the completion of whole dam body. It is noted that rockfill materials are not only non-linear but also time-dependent in the computation.

5.2. Comparison of numerical results with in situ measurements

The deformation in construction stage also includes both non-linear and time-dependent components. It is noted that the deformation and separation were monitored at the in situ measurement points as shown in Fig. 9. These in situ measurements are used to verify the numerical simulations of the contact analysis method. Fig. 10 compares the settlement in dam body and the horizontal displacement increment at the upstream slope in August 1999. This figure shows that numerical results are in good agreement with observations for both settlement and horizontal displacement increment at the upstream slope. The settlements obtained from numerical simulation are slightly bigger than the observations in lower zone but slightly smaller than the observations in the upper zones. Tables 5–7 qualitatively compare the numerical results and in situ observations. Table 5 compares the settlements at different measurement points. Table 6 compares horizontal displacement increments at four measurement points. Table 7 compares maximum opening and deficient of stage-I slab and stage-II slab. Above comparisons show that the numerical results are in good agreement with in situ measurements in construction stage. Fig. 11 gives the openings (separation) between concrete slabs and cushion layer as well as the deficient of dam body obtained from

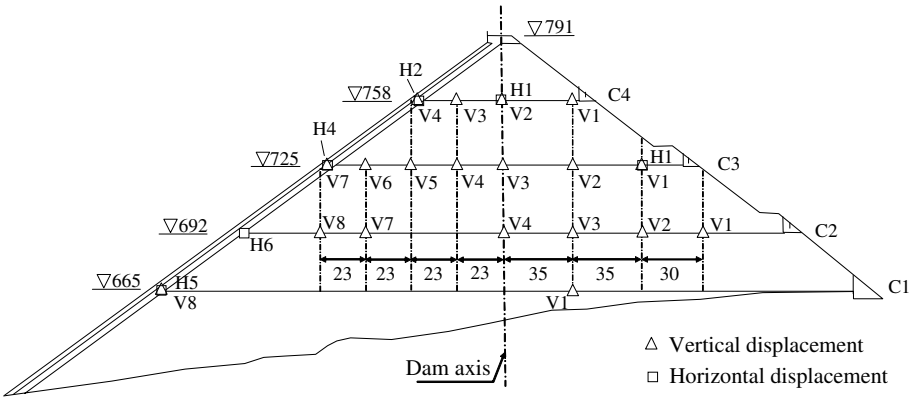

Fig. 9. Layout of in situ measurement points.

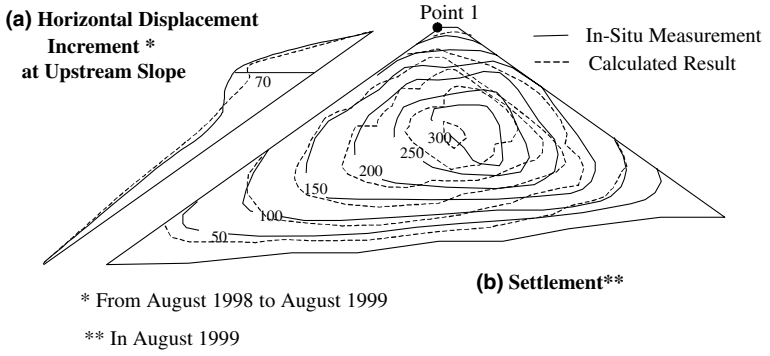

Fig. 10. Deformations obtained by numerical simulation and in situ measurement.

Table 5
Comparison of vertical settlements (as August 1999)

Points	Elevation (m)	From dam axis (m)	In situ measurement (m)	Numerical results (m)
C1-V1	665	35	1.478	1.300
C1-V8	665	−170	0.816	0.662
C2-V1	692	100	1.576	1.200
C2-V2	692	70	2.269	2.110
C3-V1	725	70	1.826	1.500
C3-V2	725	35	3.217	3.220
C3-V3	725	0	2.727	3.000
C3-V4	725	−23	2.788	2.680
C3-V5	725	−46	2.114	2.000
C3-V6	725	−69	1.562	1.480
C3-V7	725	−92	1.654	0.961
C4-V1	758	35	2.056	1.420
C4-V2	758	0	1.601	1.492
C4-V3	758	−23	1.758	1.720
C4-V4	758	−46	1.025	0.987

numerical simulations at the stage-I and stage-II slabs. The deficient and the opening are much bigger in the upper zone than in the lower zone. When the dam is high, the non-linear properties of rockfill materials heavily affect the deficient and the opening.

5.3. Development of separation and deficient with dam height

The development of the separation between stage-II slab and the cushion layer is traced when higher parts of dam body (after stage-II slab) are constructed. These parts and construction phases are shown in Fig. 12. Table 8 gives the openings calculated at each construction phase. These results show that the opening at the top of stage-II slab has already reached 31 cm wide when construction phase ① (up to El.768

Table 6
Comparison of horizontal displacement increments

Points		C1-H5	C2-H6	C3-H4	C4-H2
Increment (December 1998 to March 1999)	Numerical result (cm)	4.2	5.9	4.7	24.5
	In situ measurement (cm)	2.7	3.3	2.3	18.5
Increment (December 1998 to August 1999)	Numerical result (cm)	8.4	12.0	22.0	50
	In situ measurement (cm)	9.8	7.8	9.0	69.0

Table 7
Maximum opening and deficient

Cases	Stage-I slab			Stage-II slab		
	Opening width (m)	Opening depth (m)	Deficient (m)	Opening width (m)	Opening depth (m)	Deficient (m)
In situ measurement	0.15	7.2	0.43	0.10	5.0	1.03
Numerical results	0.13	8.0	0.45	0.40	14.0	1.00
No elevation difference scheme	0.12	7.5	0.50	0.25	13.0	0.93

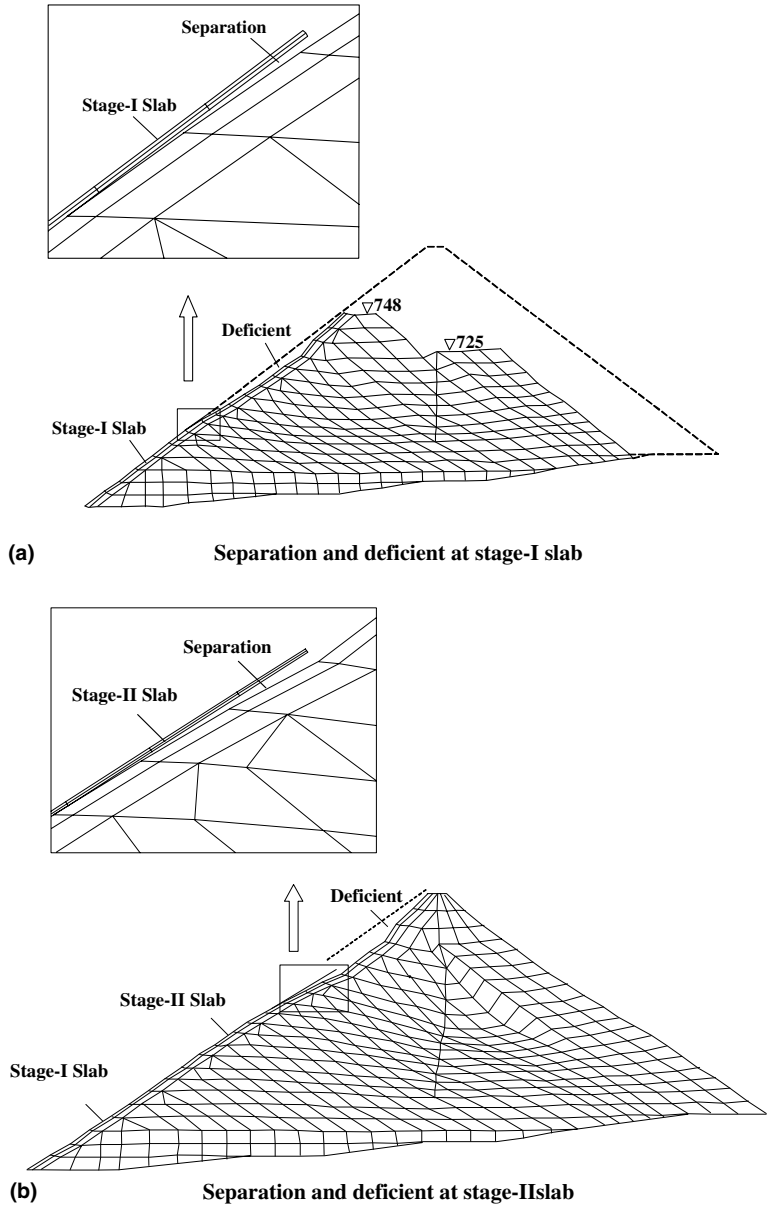

Fig. 11. Separation of concrete slab and deficient of upstream slope.

m) was completed. The self-weight of the rockfill layers adjacent to the top of the face slab is the primary factor of separation. With the reservoir impounding (construction phase ②), the face slab was gradually pressed towards the cushion layer and only the opening above the water level only remained. When the upstream water level reached El.737 m, the width of the opening at the top of stage-II slab decreased by 5.5 cm and the opening

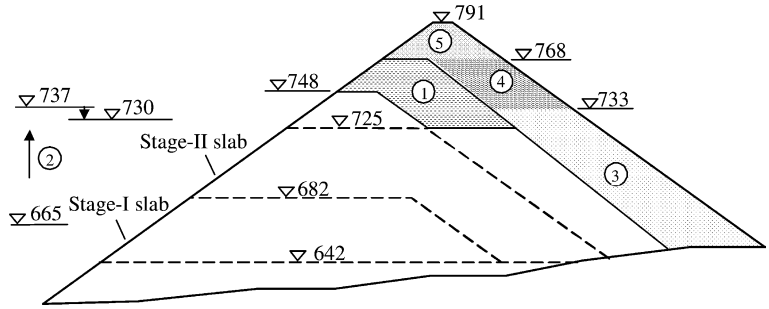

Fig. 12. Construction phases after casting stage-II slab.

Table 8
Opening between stage-II slab and dam body

Construction phase	Opening width (m)	Opening depth (m)	Maximum deficient (m)
1	0.31	13.0	0.62
2	0.26	7.5	0.69
3	0.32	13.5	0.76
4	0.36	13.5	0.84
5	0.40	14.0	1.00

depth decreased drastically. On the contrary, the construction phase ③ produced only 6 cm more opening, although this part of rockfill is approximately 80 m high. This indicates that the construction of downstream block has little influence on the opening because the block is far away from the face slab. Subsequent construction phases ④ and ⑤ cause 8 cm more opening. This again indicates that the self-weight of rockfill layers adjacent to and above the top of stage-II face slab has

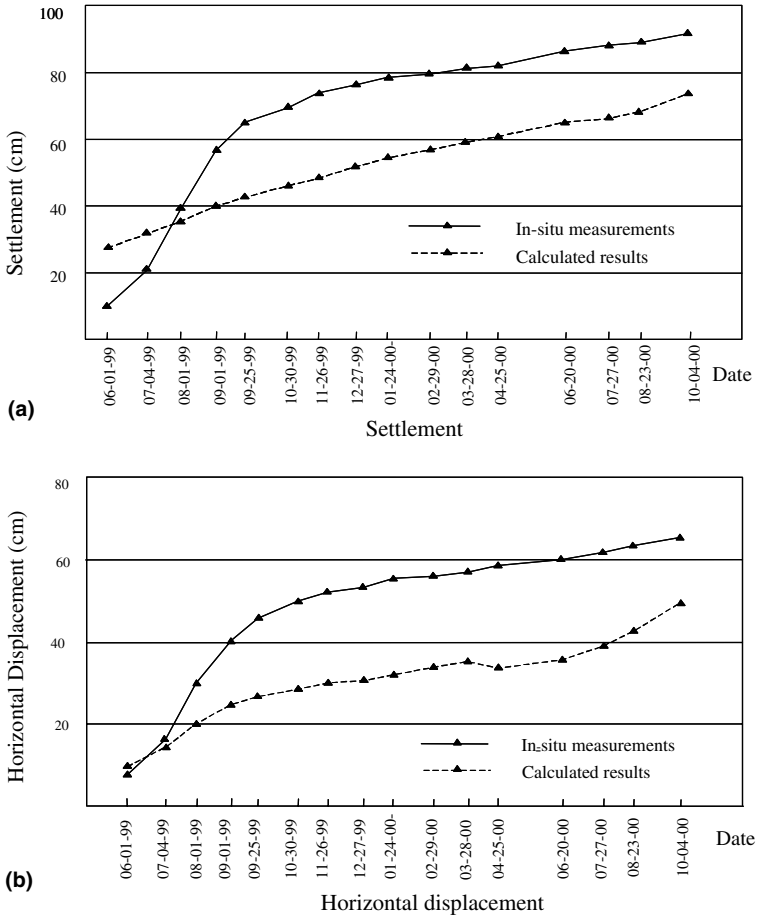

Fig. 13. Post-construction displacements at dam crest (point 1).

relatively great influence on the opening. The deficient of the cushion layer has the similar change as shown in Table 6.

5.4. No elevation difference scheme

As shown in Fig. 5(b), the dam body is not constructed by a layer-by-layer scheme. In the layer-by-layer scheme, dam body was constructed in the entire cross-section while concrete face was still cast in three stages as previous scheme. At any time, the entire cross-section has no elevation difference (thus called as no elevation difference scheme). If the dam body is constructed by the layer-by-layer scheme, what are the separation and the deficient? We divide the dam body into 26 layers, but the concrete face slabs were still cast in three stages. As pointed out in Section 5.3, reservoir filling presses the slab towards slope and the opening is reduced. The opening should be bigger if reservoir filling process is ignored. Therefore, this scheme ignores the reservoir filling and has 29 increments in computation. Table 7 also summarized the maximum opening and deficient obtained by this scheme. The results show that the openings at stage-I and stage-II slabs are smaller than those in the actual construction scheme. However, the deficient is little different. Therefore, no

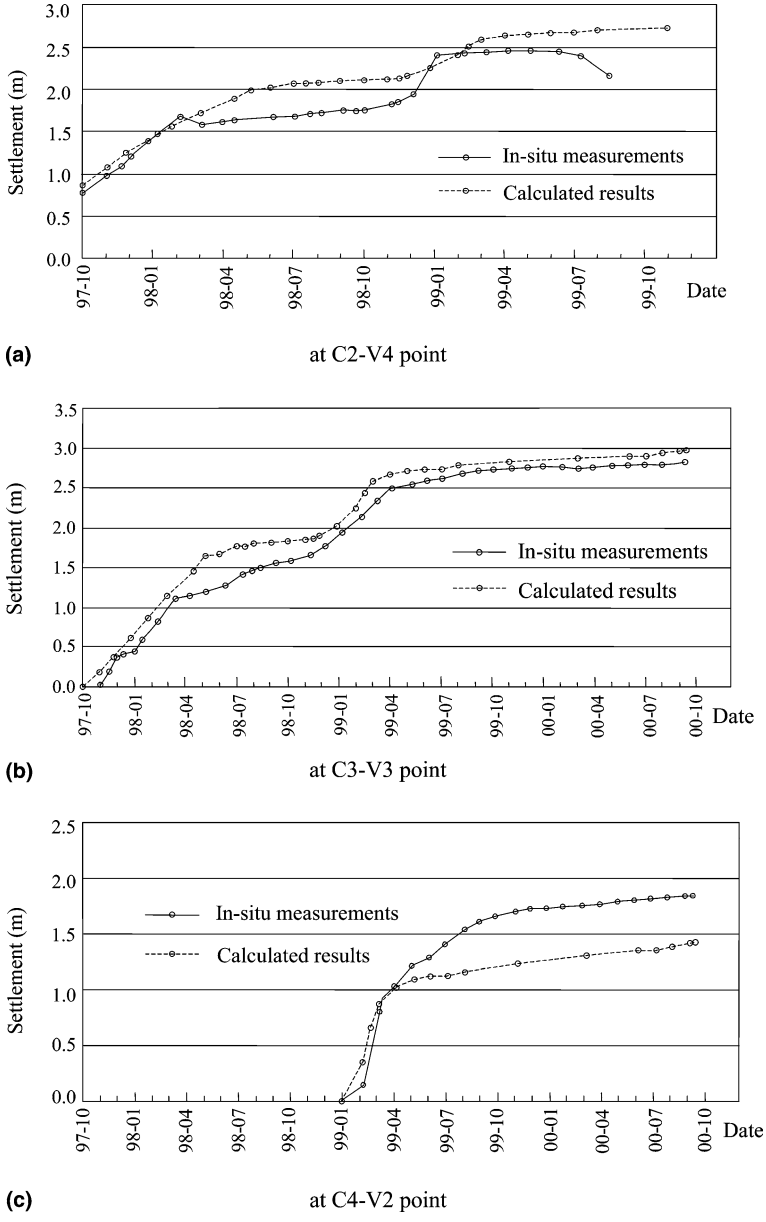

Fig. 14. Comparison of settlements along dam axis.

elevation difference scheme can reduce openings to some extent.

5.5. Time-dependent deformation during operation

Creep deformation is the main source at this stage. This stage starts from the completion of the construction of dam body (since January 1999) and ends on the October 2000 in our computation. The simulated displacements at several typical points are compared with in situ measurements. Fig. 13 compares the displacements at the dam crest mainly due to the rockfill creep behavior in the period of June 1999 to October 2000 (called post-construction displacement). Fig. 14 compares the settlements at three points along dam axis. Because the construction time is different, the date range in each figure is different. Rainfall season from June to October in 1999 introduced relative great additional deformation [21]. Because the current computational model does not take wetting deformation into account, the numerical results are lower than the in situ measurements during this period and onward time. This can be seen from Figs. 13 and 14(c). However, the calculated deformation rate for both settlement and horizontal displacement after the rainfall season of 1999 is in good agreement with in situ measurements.

The openings and the deficient at stage-III slabs are given in Fig. 15. Table 9 lists the values of opening and maximum deficient at three stage slabs. Numerical results and in situ measurements are in good agreement except for the separation between the stage-II slab and the cushion layer. The openings for stage-I and stage-II slabs as well as the deficient of the cushion layer increased notably due to the creep deformation of dam body. It is quite evident that the separation between the stage-III slab and the cushion layer is caused alone

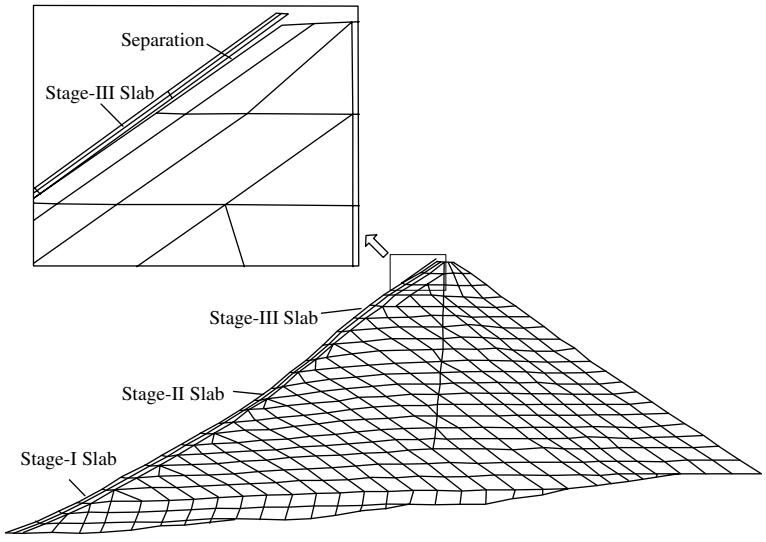

Fig. 15. Separation of concrete slab and deficient of upstream slope at stage-III slab.

Table 9
Calculated and measured results of openings and deficient (Unit: m)

Openings		Case 1	Case 2	Case 3
Stage-I Slab	Width	0.15	0.13	0.12
	Depth	7.2	9.0	7.5
Stage-II Slab	Width	0.10	0.40	0.25
	Depth	5.0	14.0	13.0
Stage-III Slab	Width	0.03	0.02	
	Depth	10.0	11.0	
Maximum deficient of upstream slope		Case 1	Case 2	Case 3
Stage-II Slab		0.43	0.45	0.50
Stage-III Slab		1.03[a]	1.00	0.93

Where Case 1 – In situ measurements
Case 2 – Numerical results including time-dependent deformation of rockfills
Case 3 – Numerical results by no elevation difference (layer by layer) scheme.
[a] −0.78 m (the actual deficient) + 0.25 m (over constructed layer).

by the post-construction deformation of dam body. In order to reduce this separation as well as the deficient, engineering measures are necessary. For example, the face slab can be cast as late as possible so that the creep deformation of dam body can take place to the greatest extent. Furthermore, the dam body is compacted with fully wetted rockfill materials to minimize the creep and wetting deformation.

6. Conclusions

A high concrete-face rockfill dam, Tianshengqiao-I project, was numerically analyzed through a contact analysis method. The deficient of dam body and the separation between concrete slab and cushion layer are numerically simulated and compared with in situ measurements. The effect of non-linearity and the creep deformation of rockfill dam body on the deficient and the separation are carefully studied in construction and operation stages. Following conclusions and understandings can be drawn from this study:

First, the proposed contact analysis method can be applied to the simulation for the separation of face slab and cushion layer whether the separation is finite or not. This method does not require any interface element along the interface, and the rockfill materials may be non-linear and time-dependent. Direct constraints along the interface can easily treat strong non-linearity of rockfill materials, separation-contact, sliding and re-separation along the interface through iterations. Numerical examples show that the current method can qualitatively and quantitatively reproduce the fundamental behaviors of the opening between cushion layer and face slabs at different stages of TSQ-I high dam.

Second, the separation between concrete face slab and dam body as well as the deficient of cushion layer are inevitable in high CFRD when the face slab is concreted in stages. The primary cause of the separation was that the previously constructed rockfill blocks, which support the face slab, produce additional vertical and horizontal deformations under the self-weight of the lately compacted rockfill blocks, but the concrete slab cannot deform harmoniously with the cushion layer due to its high stiffness. The deficient of cushion is also caused by this large vertical deformation.

Third, time-dependent deformation in operation stage will enlarge the separation on the upper face slabs as well as the deficient in the upstream slope. When water level rises, the opening of face slab and cushion may close up partially due to water pressure. However, this close-up will produce stress concentration near the toe of separation, possibly producing concentrative cracks in concrete face slabs. This may make the face slabs lose the leakage resistance.

Last, design and construction scheme can reduce the separation between concrete face and dam body as well as the deficient of the cushion layer. These engineering treatments include: (1) Well construct dam body with fully wetted rockfill materials. This can minimize the post-construction settlements of dam body. (2) Cast the concrete face slab as late as possible, so that the time-dependent deformation of the constructed dam body can take place to the greatest extent. (3) Cast the staged concrete face slab with a top elevation lower than the top of the supporting dam section. (4) Optimize temporary cross-sections to reduce elevation differences between blocks in different construction stages.

Acknowledgements

Authors would like to thank the anonymous referees whose comments helped us improve the presentation of this paper.

References

[1] Cook JB, Sherard JL, editors. Concrete face rockfill dams-Design, construction and performance. New York: ASCE; 1985.
[2] Cook JB. Rockfill and rockfill dams. In: Proceedings of International Symposium on High Earth-rockfill Dams, Beijing, Chinese Society for Hydro-electric Engineering (CSHEE), 1993. p. 104 (Invited Lecture).
[3] Yoon YS, Won JP, Woo SK, Song YC. Enhanced durability performance of fly ash concrete for concrete-faced rockfill dam application. Cem Concr Res 2002;32:23–30.
[4] Cook JB. Process in rockfill dams. The 18th Terzaghi Lecture. J Geotech Eng, ASCE 1984;110(10):1383–414.
[5] Goodman RE, Taylor RL, Brekke TL. A model for the mechanics of jointed rock. J Soil Mech Foundat Div, ASCE 1968;94(3):637–60.
[6] Kikuchi N, Oden JT. Contact problems in elasticity: A study of variational inequalities and finite element methods. Amsterdam: SIAM, Elsevier Science; 1988.
[7] Wang JG, Ichikawa Y, Leung CF. A constitutive model for rock interfaces and joints. Int J Rock Mech Min Sci 2003;40(1):41–53.
[8] Mottershead JE. Lagrange multiplier formulation for FEM. Computational methods in contact mechanics. Computational Mechanics Publications; 1993. p. 99.
[9] Yagawa G, Kanto Y. Finite element analysis of contact problems using the penalty function method. Computational methods in contact mechanics. Computational Mechanics Publications; 1993. p. 127.
[10] Karim MR, Nogami T, Wang JG. Analysis of transient response of saturated porous elastic soil under cyclic loading using element-free Galerkin method. Int J Solids Struct 2002;39(6):6011–33.
[11] Uddin N. A dynamic analysis procedure for concrete-faced rockfill dams subjected to strong seismic excitation. Comput Struct 1999;72:409–21.
[12] Justo JL, Durand P. Settlement-time behaviour of granular embankments. Int J Numer Anal Meth Geomech 2000;24:281–303.
[13] Parkin AK. Settlement rate behavior of some rockfill dams in Australia. In: Proceedings of the 11th ICSMFE, San Francisco, vol. 4, 1985. p. 2007–10.

[14] Day RA, Potts DM. Zero thickness interface elements – numerical stability and application. Int J Numer Anal Meth Geomech 1994;94(18):689–708.
[15] Luiz Paulo QT, Aurelio A, Ricardo J, Alberto Jorge A. Xingo concrete face rockfill dam behavior. Commission Int 2000:1383–402.
[16] Duncan JM, Byrne P, Wong K, Mabry P. Strength, stress–strain and bulk modulus parameters for finite element analysis of stresses and movements in soil masses. Report No. UCB/GT/80-01, University of California, Berkeley, 1980.
[17] Zhao K, Li G, Shen Z. Back analysis of field monitoring data of Tianshengqiao CFRD. J Nanjing Hyd Res Inst 2002(4):15–9. [in Chinese].
[18] Wang JG, Liu GR. A point interpolation meshless method based on radial basis functions. Int J Numer Meth Eng 2002;54(11):1623–48.
[19] Zhong ZH, Nilsson L. A contact searching algorithm for general 3-D contact-impact problems. Comput Struct 1990;34: 327–35.
[20] Zienkiewicz OC, Taylor RL. The finite element method. 5th ed.. The basis, vol. 1. Boston: Butterworth-Heinemann; 2000.
[21] Xu M. Analysis of cracks on Tianshengqiao-I concrete-faced rockfill dam. J Hongshui River 2000;3:40–7. [in Chinese].
[22] Wang JG, Nogami T, Dasari GR, Lin PZ. A weak coupling algorithm for seabed-wave interaction analysis. Comput Meth Appl Mech Eng 2004;193(36–38):3935–56.